

EUV Line Intensities of Fe X

P. R. YOUNG,¹ H. E. MASON,¹ A. K. BHATIA,²
G. A. DOSCHEK,³ AND R. J. THOMAS²

¹Department of Applied Mathematics and Theoretical Physics,
Silver Street, Cambridge CB3 9EW, UK

²Laboratory for Astronomy and Solar Physics, Code 680,
NASA-Goddard Space Flight Center, Greenbelt MD 20771, USA

³E.O. Hulburt Center for Space Research, Naval Research Laboratory,
Washington DC 20375-5000, USA

The 4 configuration, distorted wave calculation of Bhatia & Doschek (1995) (hereafter referred to as BD95), together with the ground transition calculation of Pelan & Berrington (1995) are here used to predict the intensities of the Fe X EUV lines, which are then used to derive electron densities from several solar spectra, including the recent SERTS spectra.

1. Introduction

The identification of the red coronal line as being the ground transition of Fe X helped lead to the idea of the corona as a million degree plasma. The importance of Fe X today lies in it being formed over the temperature region $8-12 \times 10^5 \text{K}$, bridging the different morphologies of the transition region and coronal plasmas.

The main EUV lines of Fe X are summarised in table 1: the $3s^23p^5 \ ^2P-3s^23p^43d \ ^2P, \ ^2D, \ ^2S$ transitions contribute over 80% of the power output of Fe X, giving rise to a complex of strong lines in the 170–190Å region; the $3s^23p^43d \ ^4D_{5/2,7/2}$ levels are barely split and decay down to the $3s^23p^5 \ ^2P_{3/2}$ level via electric dipole and magnetic *quadrupole* transitions, respectively, giving rise to a self-blended line observed at 257.26Å.

2. Atomic Data

2.1. Radiative Data and Energy Levels

A 13 configuration model of Fe X was used in the radiative code SUPERSTRUCTURE (Eissner et al. 1974), to produce transition probabilities and energy levels. The transition probabilities were found to be within 5% of those of Fawcett (1991). Observed energy levels from Corliss & Sugar (1982) and Jupén et al. (1994), were used together with scaled SUPERSTRUCTURE energies for the remaining levels.

2.2. Electron Excitation Data

Mason (1994) assessed the (then) available electron collisional excitation data for Fe X. Subsequently, a Distorted Wave calculation has been done by BD95 for 5 values of the incoming electron energy for a four configuration model of Fe X. This calculation is compared with two previous calculations in Figure 1 (left frame), where the *reduced†* collision strength is plotted against the reduced energy for the strong transition that gives rise to the 174.53Å line.

The high energy limit point at $E_r = 1$ can be accurately determined for allowed transitions using oscillator strengths from, e.g., SUPERSTRUCTURE via the expression $4\omega f/\Delta E$. This allows a crude comparison of the calculations—the BD95 results are

† see Burgess & Tully (1992) for details

TABLE 1. Important Fe X lines and their associated transitions. Note that, for Fe X, $^2P_{3/2}$ is the ground level and $^2P_{1/2}$ is the first excited level.

Upper Level Configuration	Upper Level Term	Lower Level Configuration	Lower Level Term	Wavelength (Å)
$3s3p^6$	$^2S_{1/2}$	$3s^23p^5$	$^2P_{3/2}$	345.72
$3s^23p^43d$	$^4D_{5/2,7/2}$		$^2P_{3/2}$	257.26
	$^2D_{5/2}$		$^2P_{3/2}$	174.53
	$^2P_{3/2}$		$^2P_{3/2}$	177.24
	$^2S_{1/2}$		$^2P_{3/2}$	184.54
	$^2D_{3/2}$		$^2P_{1/2}$	175.27

$\sim 20\%$ more accurate than the Mann (1983) results due to the inclusion of the $3s3p^53d$ configuration, but a further $\sim 20\%$ improvement is still possible. This can largely be achieved by including the $3s^23p^33d^2$ configuration (Nussbaumer, 1976).

2.3. Resonance Structure in the Ground Transition

BD95 did not include any resonance structure in their model, which is particularly important for the ground $^2P_{3/2}-^2P_{1/2}$ transition. This calculation has been done separately by Pelan & Berrington (1995), and the two are compared in figure 1 (right frame), together with the results of Mohan et al. (1994). Although this latter R-matrix calculation included some resonance structure, the fine-structure cross-section below the first excited state was not calculated (Pelan, private communication).

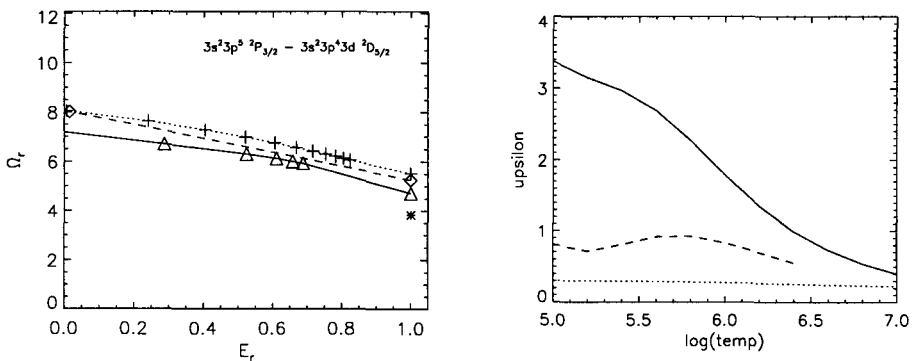


FIGURE 1. The left frame shows the reduced collision strength for the Fe X transition that gives rise to the 174.53 Å line. The three sets of points represent the results of BD95 (Δ), Mason 1975 (\diamond) and Mann 1983 (+). * represents the accurate high energy limit point, and $E_r = 0$ corresponds to the threshold energy of the transition. The right frame compares the thermally-averaged collision strengths for the ground $^2P_{3/2}-^2P_{1/2}$ transition obtained by: Pelan & Berrington (—); Mohan et al. (---); Bhatia & Doschek (.....).

3. Density Diagnostics

In the 170–190 Å region, three density diagnostics are formed by taking the ratio of the 174.53, 177.24 and 184.54 Å lines relative to the 175.27 Å line. The new results for one

TABLE 2. Intensity ratios for the 175.27Å line taken relative to the 174.53, 177.24, 184.54 lines; the figure in brackets is the derived density. The observations used are: ¹Malinovsky & Heroux (1972); ²Behring et al. (1976); ³Dere et al. (1979); ⁴Drake et al. (1995). (This latter spectrum is of the star Procyon, observed by EUVE—the 184.54Å line was observed in a different bandpass and so the derived density is less certain.)

Line	Full Disk Sun ¹	Full Disk Sun ²	Solar Flare ³	Procyon ⁴
174.53	0.085 (8.7)	0.18 (9.3)	0.5 (10.7)	0.16 (9.2)
177.24	0.16 (8.8)	0.26 (9.2)	0.4 (9.5)	0.30 (9.3)
184.54	0.41 (8.8)	0.6 (9.1)	n/a	0.92 (9.5 ?)

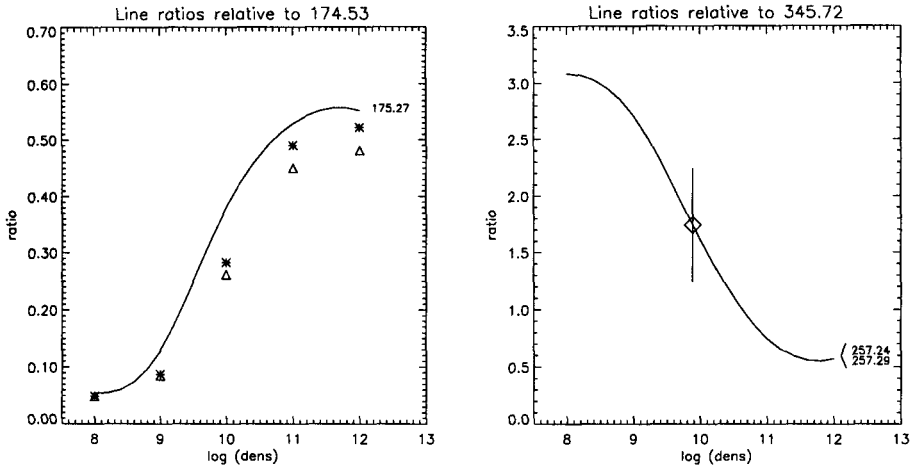


FIGURE 2. The left frame shows the new results presented here for the 175.27/174.53 ratio (solid line). The Δ are the same results but with the BD95 collision strength for the ground transition, while the * are the results of Brickhouse et al. (1994), who used the collision strengths of Mann for the transition shown. The right frame shows the 257.26/345.72 ratio with SERTS intensities and error bars marked on (note: theory splits the 257.26 blend into lines at 257.24, 29Å).

of these ratios are presented in figure 2 (left frame), and used to derive the densities in table 2 for various spectra.

The 257.26/345.72 ratio is the only other useful density diagnostic in the EUV for Fe X and was observed by the Solar EUV Rocket Telescope and Spectrograph (SERTS) flight of 1989.

4. Results from SERTS

4.1. Densities Derived from Fe X

Figure 2 (right frame) shows the density obtained from the SERTS spectrum of Thomas & Neupert (1994) using the Fe X 257.26 and 345.72 Å lines. However this spectrum has been spatially-averaged over a region containing considerable inhomogeneities.

The variation of the SERTS emission over the slit of the spectrograph for the Fe X 257.26Å, 345.72Å, and Fe XVI 335.40Å lines is shown in figure 3. It can be seen that the subflare (seen clearly near the centre of the slit in the Fe XVI line), gives different

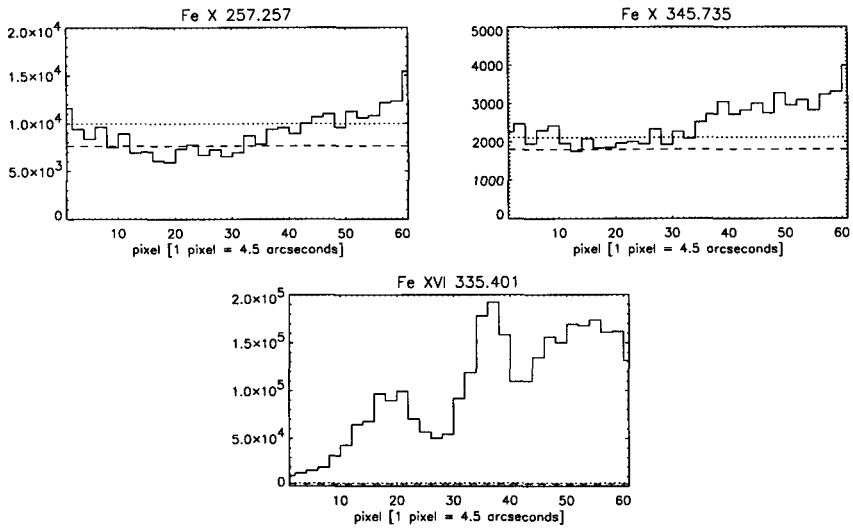


FIGURE 3. Spatial variation across the SERTS slit of Fe X 257.26 Å and 345.72 Å (seen at 345.735 Å by SERTS), and Fe XVI 335.40 Å. The dashed line represents the average background, while the dotted line represents the 1σ variation of the background.

TABLE 3. Densities derived from the SERTS spectrum for various ions formed around 10^6 K. The collisional data for Mg VIII and Si X are from Zhang et al. (1994) and this, together with the radiative data were supplied by K. P. Dere.

Ion	T_{max}	Ratio	Density	Data Source
Mg VIII	5.9	436.73/430.45	$5.0 \times 10^8?$	present
Si VIII	5.9	276.85/319.84	2.5×10^{10}	Dwivedi (1994)
Fe X	6.0	257.26/345.72	8.9×10^9	present
Si IX	6.0	349.87/345.13	$\gtrsim 10^{10}$	Mason & Bhatia (1978)
Si X	6.1	356.03/347.41	$1.3 \times 10^9?$	present

contributions to the two Fe X lines. One can estimate the subflare 257.26/345.72 ratio as ≈ 1.2 and the active region loops (to the right of the subflare) ratio as ≈ 2.5 , leading to densities $\approx 2.5 \times 10^{10}$ and $\approx 2.0 \times 10^9$, respectively.

4.2. Comparison with Other Ions

An important study for both solar and atomic physics is to check if ions with similar temperatures of peak abundance (T_{max}) give consistent results for the electron density. For Fe X, with T_{max} around 1×10^6 K, we have Si VIII–X and Mg VIII, all with useful density diagnostics lying within the SERTS wavelength range.

The densities predicted by these diagnostics are shown in table 3 where one can see a fair degree of scatter. However the Mg VIII ratio is only sensitive to densities $\lesssim 10^9$, and the error bars are large enough to make this density estimate highly uncertain. The Si X ratio involves the 347.41 Å line which was marred by a plate flaw (Thomas & Neupert, 1994), again making the density estimate uncertain.

TABLE 4. Wavelength bands in Å covered by CDS

NIS	308–381		513–633	
GIS	151–221	256–338	393–493	656–785

5. Future Observations

The SERTS rocket will be flown again in the spring of 1995, with a new multilayer-coated grating tuned to enhance the spectral region between 170–220Å. This should allow the full set of Fe X diagnostics to be observed in that wavelength range for the first time ever from individual solar features.

In addition, the *Solar and Heliospheric Observatory (SOHO)*, to be launched in October 1995, will contain several instruments including the Coronal Diagnostic Spectrometer (CDS) which will cover the EUV region of the solar spectrum. CDS's two spectrometers (the grazing incidence, GIS, and the normal incidence, NIS) will cover most of the 150–800Å region in the bands shown in table 4.

As can be seen, the 170–190Å lines will all be observed, together with the 257.26 blend and the 345.72 line. However, these latter two lines are covered separately by the GIS and NIS, respectively, and so the ratio will be subject to calibration uncertainties.

The 345.72 and 174.53 lines may be used to help cross-calibrate the GIS and NIS since the 345.72/174.53 ratio is relatively density and temperature insensitive over $\log T = 6.0 \pm 0.15$ and $\log N_e \sim 8 - 10$, with values 0.02–0.05.

PRY and HEM acknowledge the support of EPSRC and PPARC, respectively.

REFERENCES

- BEHRING, W. E., COHEN, L., FELDMAN, U., & DOSCHEK, G. A. 1976, *ApJ*, 203, 521
 BHATIA, A. K. & DOSCHEK, G. A. 1995, *ADNDT*, in press
 BRICKHOUSE, N. S., RAYMOND, J. C., & SMITH, B. W. 1995, *ApJS*, in press
 BURGESS, A. & TULLY, J. A. 1992, *A&A*, 254, 436
 CORLISS, C. & SUGAR, J. 1982, *J. Phys. Chem. Ref. Data*, 11, 1
 DERE, K. P., MASON, H. E., WIDING, K. G., & BHATIA, A. K. 1979, *ApJS*, 40, 341
 DRAKE, J. J., LAMING, J. M., & WIDING, K. G. 1995, *ApJ*, 443, 393
 DWIVEDI, B. N. 1994, *Sol. Phys.*, 153, 199
 EISSNER, W., JONES, M., & NUSSBAUMER, H. 1974, *Comp. Phys. Comm.*, 8, 270
 FAWCETT, B. C. 1991, *ADNDT*, 47, 319
 JUPÉN, C., ISLER, R. C., & TRABERT, E. 1994, *MNRAS*, 264, 627
 MALINOVSKY, M. & HEROUX, L. 1973, *ApJ*, 181, 1009
 MANN, J. B. 1983, *ADNDT*, 29, 407
 MASON, H. E. 1975, *MNRAS*, 170, 651
 MASON, H. E. 1994, *ADNDT*, 57, 305
 MASON, H. E. & BHATIA, A. K. 1978, *MNRAS*, 184, 423
 MOHAN, M., HIBBERT, A., & KINGSTON, A. E. 1994, *ApJ*, 434, 389
 NUSSBAUMER, H. 1976, *A&A*, 48, 93
 PELAN, J., & BERRINGTON, K. A. 1995, *A&AS*, in press
 THOMAS, R. J. & NEUPERT, W. M. 1994, *ApJS*, 91, 461
 ZHANG, H. L., GRAZIANI, M., & PRADHAN, A. K. 1994, *A&A*, 283, 319